Supporting Information

Palladium Nanoparticles Immobilized on Nitride Carbon-Coated Mesoporous Tungsten Oxide for Formic Acid Dehydrogenation

Shengyu Du, [a] *Chenjun Zhang,* [a] *Pingping Jiang,* [a] *Yan Leng* *,[a]

[a] The Key Laboratory of Synthetic and Biological Colloids, Ministry of Education, School of Chemical and Material Engineering, Jiangnan University, Wuxi, Jiangsu 214122, China. E-mail: yanleng@jiangnan.edu.cn

Materials

Palladium chloride ($PdCl_2$, 99.9%, Alfa Aesar), Dicyandiamide ($C_2H_4N_4$, 99%, Shanghai Chemical Reagent), Formic acid (FA, HCOOH, 98%, Shanghai Chemical Reagent), Sodium formate (SF, HCOONa, 99.99%, Aladdin), Tungsten chloride (WCl_6, 99%, Aladdin), Sodium borohydride ($NaBH_4$, Shanghai Chemical Reagent), Triblock copolymer (Pluronic F127, EO_{106}-PO_{70}-EO_{106}, EO: ethylene oxide, PO: propylene oxide, Mw=12600, Sigma). All chemicals were commercially available and used directly.

Preparation of nonporous WO_3 and NC-coated nonporous WO_3

Seven mL of 65% nitric acid was diluted in deionized water (30 mL) with stirring for 10 min. $NaWO_4 \cdot 2H_2O$ (2 g, 6.1 mmol) was dissolved in 30 mL of deionized water with ultrasonic treatment for 5 min and slowly added to the nitric acid solution, which finally gave rise to a

light yellow precipitate. After stirring for another 30 min, the suspension was hydrothermally treated at 180 ^{o}C for 3 h. After cooling to room temperature, yellow product was centrifuged, washed with deionized water for 4 times and dried in vacuum for 12 h to yield about 1.2 g of the nonporous WO_3.

Dicyandiamide (DCA) (3 g, 35.7 mmol) was dissolved in hot deionized water and WO_3 (1 g, 4.3 mmol) was added into it with vigorous stirring at 70 ^{o}C for 12 h. On completion, water was removed by rotary evaporation and the solid was dried in vacuum condition (60 ^{o}C) for 12 h to give a mixture product (DCA-WO_3). 1.5 g of the hybrid was placed in an alumina boat in a quartz tube furnace and heated under argon at 400 ^{o}C for 2 h at a heating rate of 2 ^{o}C/min. After the system cooled down naturally, 0.89 g of NC_{400}@nonporous-WO_3 was obtained.

Characterization

The nitrogen sorption isotherms and pore size distribution curves were measured at the liquid nitrogen temperature (77 K) using a BELSORP-MINI analyzer. The morphology and the elemental distribution were studied by a field emission scanning electron microscope (FESEM; Hitachi S-4800, accelerated voltage: 5 kV) accompanied by Energy dispersive X-ray spectrometry (EDS; accelerated voltage: 20 kV). Scanning electron microscopy (SEM) images were performed on a SUPERSCAN SSX-550 electron microscope. Transmission electron microscopy (TEM) images were recorded with a JEOL JEM-2100 electron microscope operated at 200 kV. XRD patterns were collected on the Bruker D8 Advance powder diffractometer using Ni-filtered Cu/Kα radiation source at 40 kV and 20 mA, from 5 ° to 90 ° with a scan rate of 2 °/min. Raman analysis was performed on a PerkinElmer-Raman Station

400F spectrometer equipped with a liquid N_2 cooled charge-coupled device detector and a confocal microscope. A 350 mW near-infrared 785 nm laser was used for analysis under ambient conditions. TGA was performed on a STA409 instrument in N_2 at a heating rate of 10 °C/min. Inductively coupled plasma atomic emission spectroscopy (ICP-AES) analysis for Pd loading amount was determined by a Jarrell-Ash 1100 ICP-AES spectrometer. FT-IR spectra were carried out with a Nicolet 360 FT-IR instrument (KBr discs) in the 4000-400 cm-1 region. X-ray photoelectron spectroscopy (XPS) was conducted on a PHI 5000 Versa Probe Xray photoelectron spectrometer equipped with Al-Ka radiation (1486.6 eV).

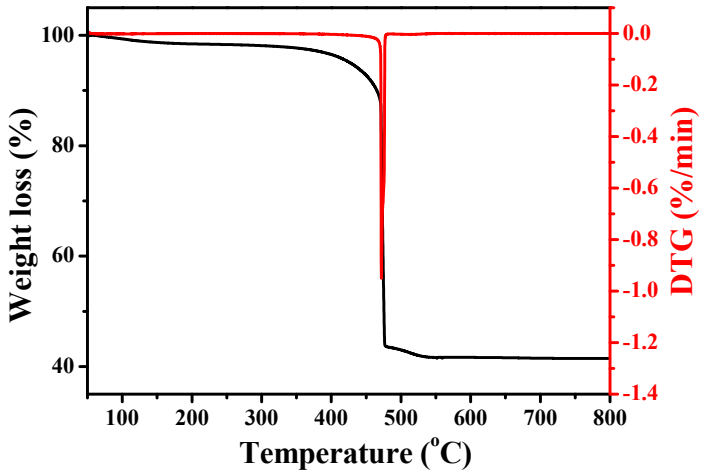

Figure S1. TGA for Pd/ NC_{400}@WO_3 in O_2.

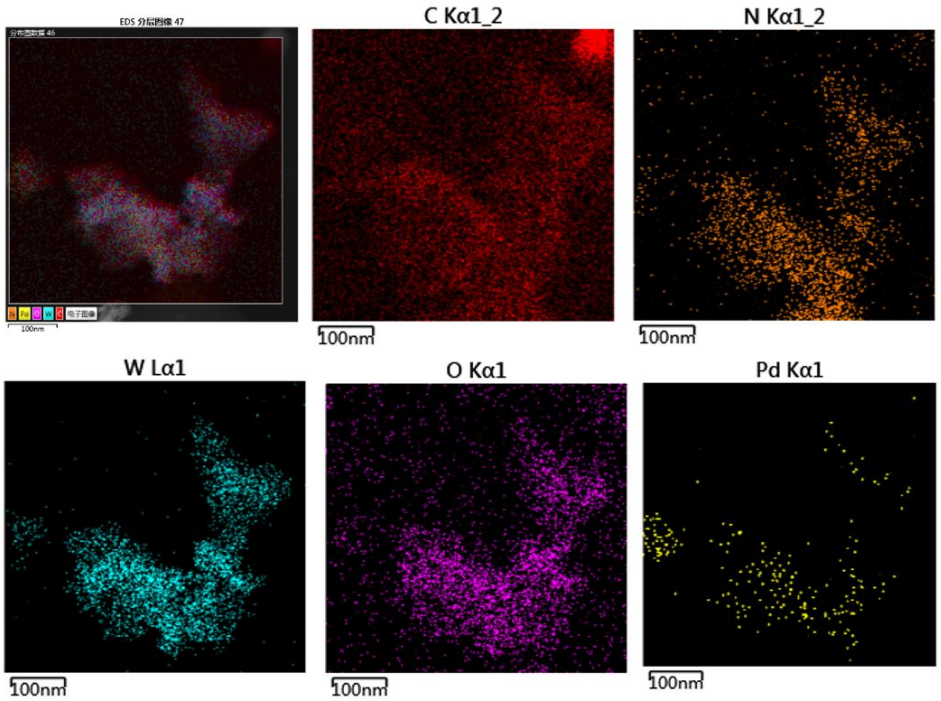

Figure S2. EDS mapping images of C, N, W, O, and Pd elements for Pd/NC_{400}@WO_3.

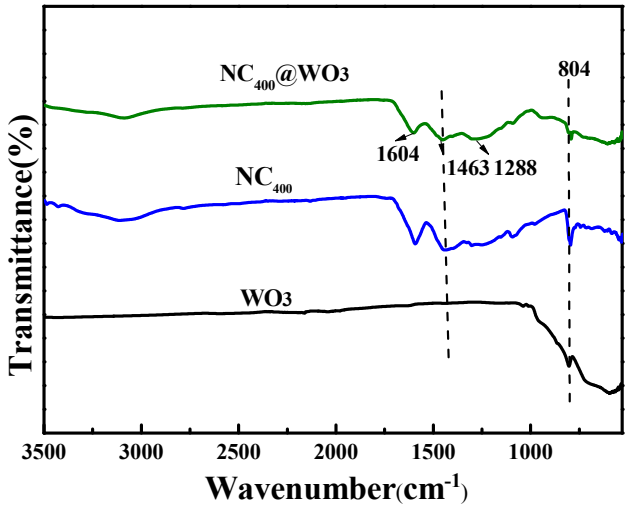

Figure S3. FT-IR spectra of WO_3, NC_{400} and NC_{400}@WO_3.

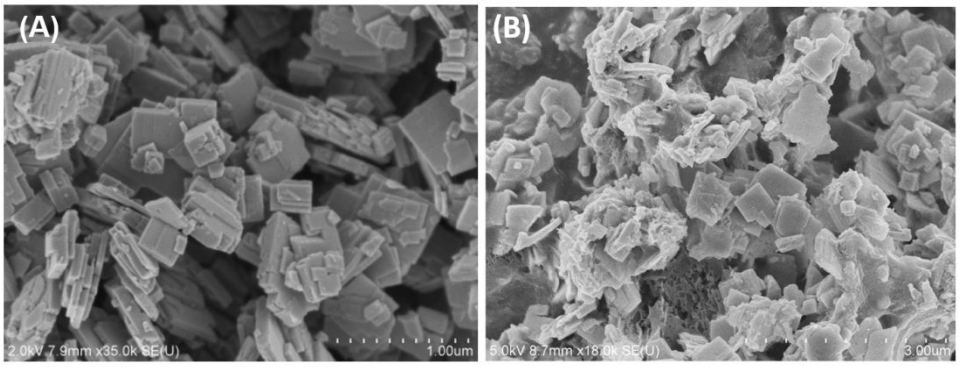

Figure S4. SEM images of (A) nonporous WO_3 and (B) NC_{400}@nonporous-WO_3.

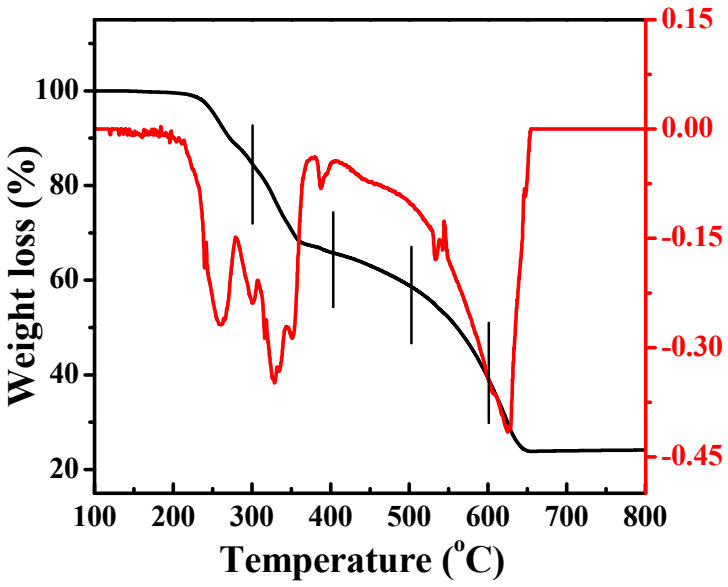

Figure S5. TGA for DCA-WO_3

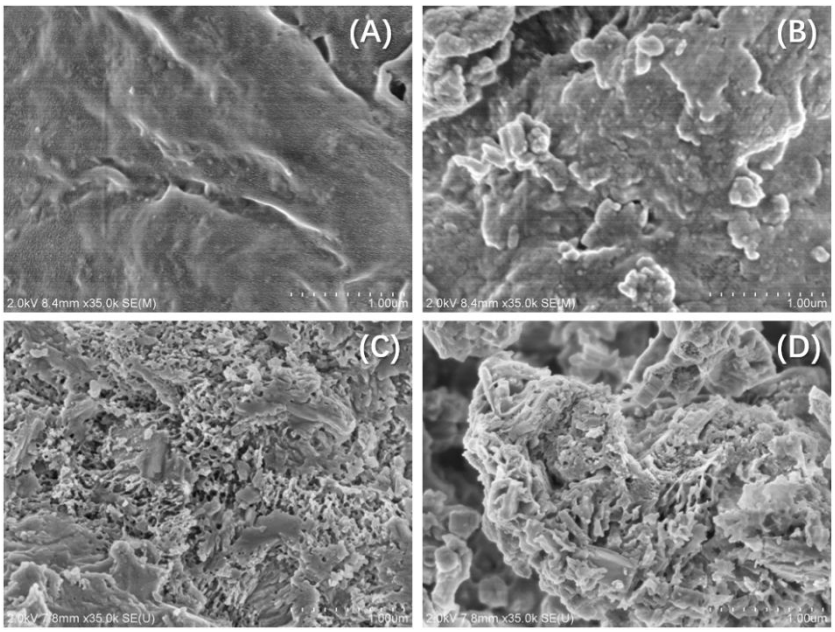

Figure S6. SEM images of (A) Pd/NC_{300}@WO_3, (B) Pd/NC_{400}@WO_3, (C) Pd/NC_{500}@WO_3 and (D) Pd/NC_{600}@WO_3

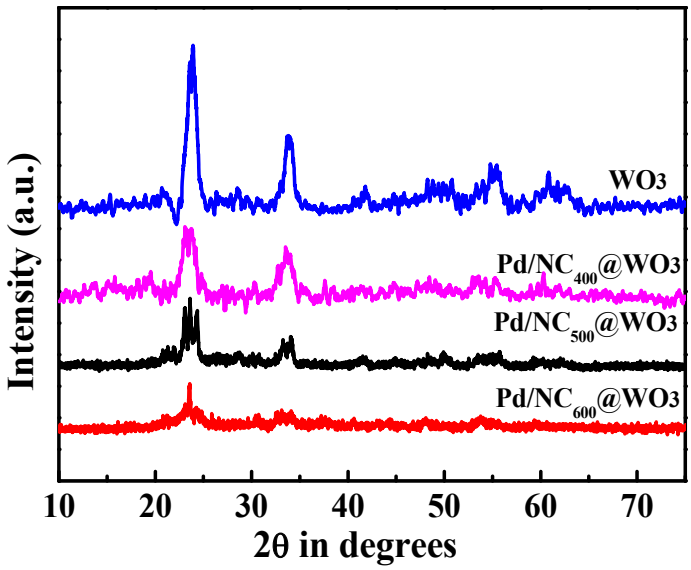

Figure S7. XRD patterns of WO_3, Pd/NC_{400}@WO_3, Pd/NC_{500}@WO_3 and Pd/NC_{600}@WO_3.

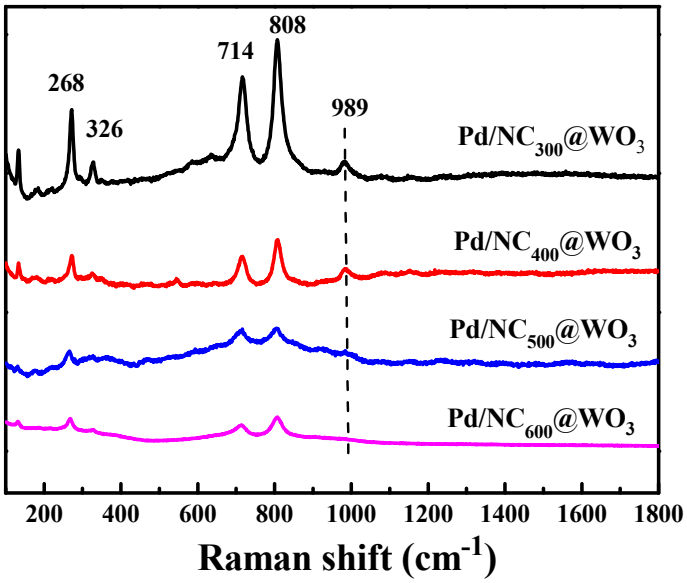

Figure S8. Raman patterns of $Pd/NC_{300}@WO_3$, $Pd/NC_{400}@WO_3$, $Pd/NC_{500}@WO_3$ and $Pd/NC_{600}@WO_3$.

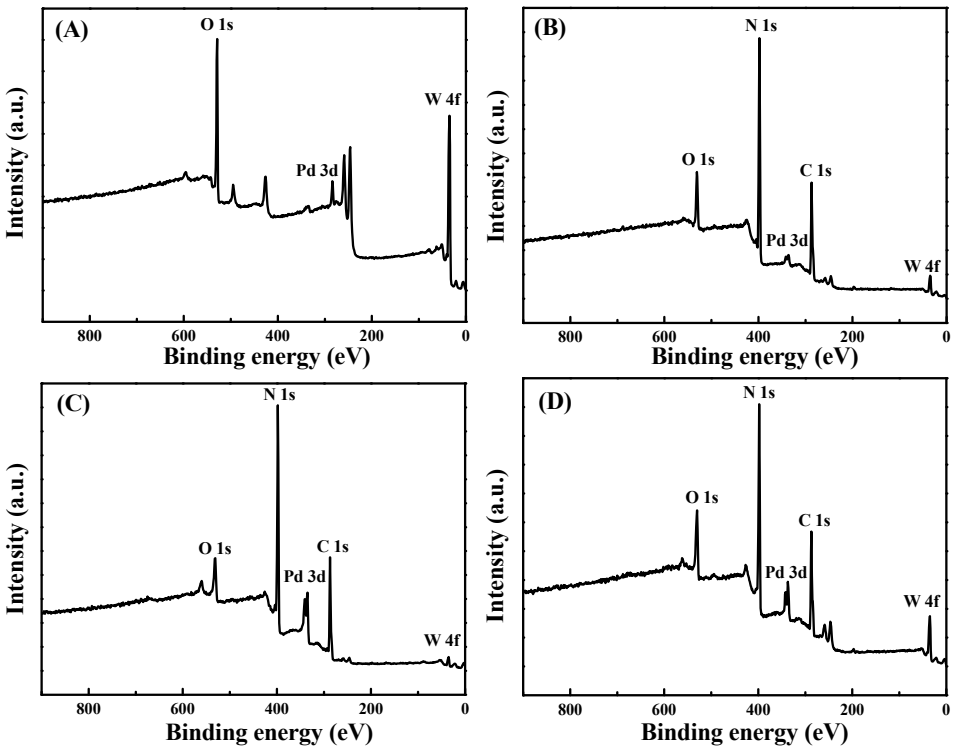

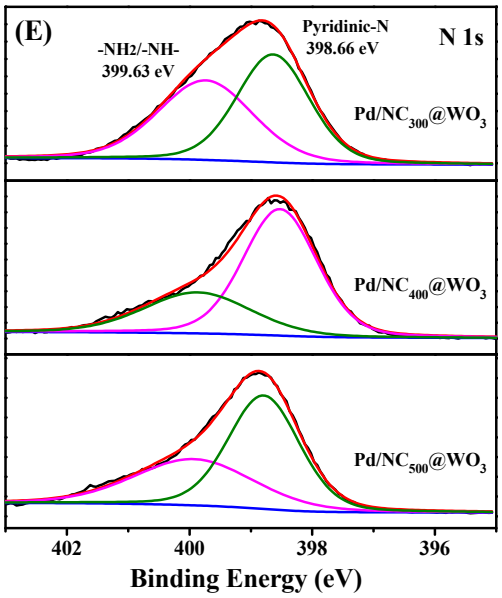

Figure S9. XPS spectra of (A) $Pd/NC_{300}@WO_3$, (B) $Pd/NC_{400}@WO_3$, (C) $Pd/NC_{500}@WO_3$ and (D) $Pd/NC_{600}@WO_3$; and (E) high resolution XPS spectra.

Table S1. the XPS signal positions and assignments for Pd 3d, W 4f, and O 1s in $Pd/NC_n@WO_3$

Sample	Pd^0 (eV)		Pd^{2+} (eV)		Pd^0/Pd^{2+} Area ratio	W^{5+}		W^{6+}		W^{5+}/W^{6+} Area ratio	C-O	Oxygen deficiency	Lattice oxygen	Pyridinic N
	$3d_{3/2}$	$3d_{5/2}$	$3d_{3/2}$	$3d_{5/2}$		$4f_{5/2}$	$4f_{7/2}$	$4f_{5/2}$	$4f_{7/2}$					
Pd/WO_3	340.66	335.43	343.23	337.83	1.26	-	-	37.71	35.58	-	-	532.18 (24.1%)	530.41 (75.9%)	-
$Pd/NC_{300}@WO_3$	341.34	335.85	343.52	336.83	1.15	36.83	35.02	37.72	35.57	0.43	533.41 (17.9%)	532.08 (50.9%)	530.65 (31.2%)	398.66 (51.1%)
$Pd/NC_{400}@WO_3$	340.85	335.69	342.96	337.38	1.90	37.38	35.21	38.04	35.82	0.52	535.88 (35.9%)	532.74 (39.0%)	530.97 (25.1%)	398.40 (68.8%)
$Pd/NC_{500}@WO_3$	341.89	336.77	343.61	336.23	0.99	36.23	35.09	37.87	35.69	0.57	542.92 (21.5%)	532.74 (38.4%)	530.51 (26.1%)	398.80 (59.3%)

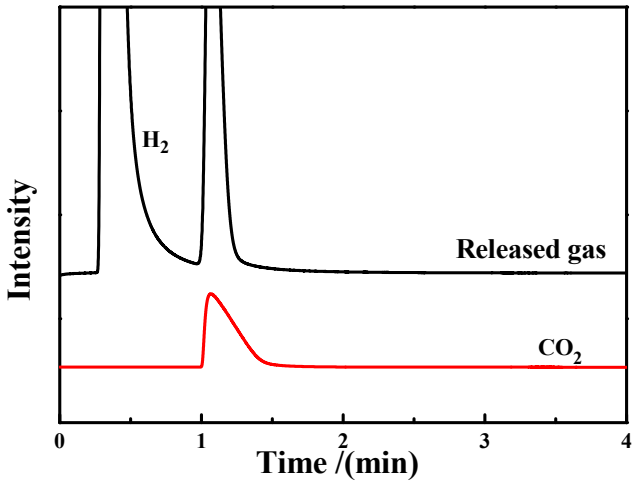

Figure S10. Gas chromatograms of the release gas from the decomposition of FA in a FA-SF system over $Pd/NC_{400}@WO_3$.

Table S2. Comparison of activities of different catalysts for hydrogen generation of FA

Entry	Catalyst	T (K)	n_{FA}/n_{metal}	TOF(h^{-1})	Ref.
1	$Co_{0.30}Au_{0.35}Pd_{0.35}/C$	298	50	80	S1
2	$Pd/mpg\text{-}C_3N_4$	298	225	114	S2
3	$Ag_{18}Pd_{82}@ZIF\text{-}8$	353	32	580	S3
4	$Ag_1Pd_4@NH_2$-UiO-66	353	100	893	S4
5	$Pd/CN_{0.25}$	298	133	752	S5
6	$Au@SiO_2$	403	-	958	S6
7	Pd/C	333	250	87	S7
8	$NiPd/NH_2$-N-rGO	298	50	954	S8
9	4-PySI-Pd@Cu(BDC)	293	-	412	S9

10	$Pd/NC_{400}@WO_3$	323	243	1225	This work

References

S1. Wang, Z. L.; Yan, J. M.; Ping, Y.; Wang, H. L.; Zheng, W. T.; Jiang, Q. An Efficient CoAuPd/C Catalyst for Hydrogen Generation from Formic Acid at Room Temperature. *Angew. Chem., Int. Ed.* **2013**, *52*, 4406-4409.

S2. Lee, J. H.; Ryu, J.; Kim, J. Y.; Nam, S. W.; Han, J. H.; Lim, T. H.; Gautam, S.; Chae, K. H.; Yoon, C. W. Carbon Dioxide Mediated, Reversible Chemical Hydrogen Storage Using a Pd Nanocatalyst Supported on Mesoporous Graphitic Carbon Nitride. *J. Mater. Chem. A.* **2014**, *2*, 9490-9495.

S3. Dai, H. M.; Xia, B. Q.; Wen, L.; Du, C.; Su, J.; Luo, W.; Cheng, G. Z. Synergistic Catalysis of AgPd@ZIF-8 on Dehydrogenation of Formic Acid. *Appl. Catal. B. Environ.* **2015**, *165*, 57-62.

S4. Gao, S. T.; Liu, W. H.; Feng, C.; Shang, N. C.; Wang, C. A Ag–Pd Alloy Supported on an Amine-Functionalized UIO-66 as an Efficient Synergetic Catalyst for the Dehydrogenation of Formic Acid at Room Temperature. *Catal. Sci. Technol.* **2016**, *6*, 869-874.

S5. Bi, Q. Y.; Lin, J. D.; Liu, Y. M.; He, H. Y.; Huang, F. Q.; Cao, Y. Dehydrogenation of Formic Acid at Room Temperature: Boosting Palladium Nanoparticle Efficiency by Coupling with Pyridinic-Nitrogen-Doped Carbon. *Angew. Chem., Int. Ed.* **2016**, *55*, 11849-11853.

S6. Mielby, J.; Kunov-Kruse, A. J.; Kegnæs, S. Decomposition of Formic Acid over Silica Encapsulated and Amine Functionalised Gold Nanoparticles. *J. Catal.* **2017**, *345*, 149-156.

S7. Jeon, H. J.; Chung, Y. M. Hydrogen Production from Formic Acid Dehydrogenation over Pd/C Catalysts: Effect of Metal and Support Properties on the Catalytic Performance. *Appl. Catal. B: Environ.* **2017**, *210*, 212-222.

S8. Yan, J. M; Li, S. J.; Yi, S. S.; Wulan, B. R.; Zheng, W. T.; Jiang, Q. Anchoring and Upgrading Ultrafine NiPd on Room-Temperature-Synthesized Bifunctional NH_2-N-RGO toward Low-Cost and Highly Efficient Catalysts for Selective Formic Acid Dehydrogenation. *Adv. Mater.* **2018**, *30*, 1703038.

S9. Alamgholiloo, H.; Zhang, S. B.; Ahadi, A.; Rostamnia, S.; Banaei, R.; Li, Z. C.; Liu, X.; Shokouhimehr, M. Synthesis of Bimetallic 4-Pysi-Pd@Cu(BDC) via Open Metal Site Cu-MOF: Effect of Metal and Support of Pd@Cu-MOFs in H_2 Generation from Formic Acid. *Molecular Catalysis* **2019**, *467*, 30-37.